J. metamorphic Geol., 2004, **22,** 395–412 doi:10.1111/j.1525-1314.2004.00522.x

Inverted metamorphic sequence in the Sikkim Himalayas: crystallization history, *P–T* gradient and implications

S. DASGUPTA[1], J. GANGULY[2] AND S. NEOGI[3]
[1]*Department of Geological Sciences, Jadavpur University, Kolkata 700 032, India*
[2]*Department of Geosciences, University of Arizona, Tucson 85721, AZ, USA (ganguly@geo.arizona.edu)*
[3]*Central Petrology Laboratory, Geological Survey of India, Kolkata 700 016, India*

ABSTRACT The metapelitic rocks of the Sikkim Himalayas show an inverted metamorphic sequence (IMS) of the complete Barrovian zones from chlorite to sillimanite + K-feldspar, with the higher grade rocks appearing at progressively higher structural levels. Within the IMS, four groups of major planar structures, S_1, S_2 and S_3 were recognised. The S_2 structures are pervasive throughout the Barrovian sequence, and are sub-parallel to the metamorphic isograds. The mineral growth in all zones is dominantly syn-S_2. The disposition of the metamorphic zones and structural features show that the zones were folded as a northerly plunging antiform. Significant bulk compositional variation, with consequent changes of mineralogy, occurs even at the scale of a thin section in some garnet zone rocks. The results of detailed petrographic and thermobarometric studies of the metapelites along a roughly E–W transect show progressive increase of both pressure and temperature with increasing structural levels in the *entire* IMS. This is contrary to all models that call for thermal inversion as a possible reason for the origin of the IMS. Also, the observation of the temporal relation between crystallization and S_2 structures is problematic for models of post-/late-metamorphic tectonic inversion by recumbent folding or thrusting. A successful model of the IMS should explain the petrological coherence of the Barrovian zones and the close relationship of crystallization in each zone with S_2 planar structures along with the observed trend(s) of *P–T* variation in Sikkim and in other sections. A discussion is presented of some of the available models that, with some modifications, seem to be capable of explaining these observations.

Key words: Himalayas; inverted Barrovian zones; main central thrust; thermobarometry; zoning in garnet.

INTRODUCTION

Over the entire length of the Himalayas, the Barrovian sequence of metamorphic isograds has been inverted in that the higher grade rocks appear at progressively higher structural levels. The origin of this inverted metamorphic sequence (IMS) has been one of the most debated topics in Himalayan geology as discussed, for example, by Hodges (2000) and Vannay & Grasemann (2001). The resolution of this problem is of fundamental importance to the understanding of the tectono-metamorphic evolution of the Himalayas. Of critical importance in this respect is the nature of *P–T* gradient in the IMS since any thermo-tectonic model has a predictable consequence about the peak metamorphic *P–T* gradient or metamorphic field gradient (i.e. peak temperature *v*. pressure at the peak temperature).

Numerous thermobarometric studies have been undertaken in different sections of the IMS (e.g. Hodges & Silverberg, 1988; Hubbard, 1989; Inger & Harris, 1992; McFarlane, 1995; Vannay & Hodges, 1996; Vannay & Grasemann, 1998; Vannay *et al.*, 1999; Fraser *et al.*, 2000; Stephenson *et al.*, 2000; Catlos *et al.*, 2001; Kohn *et al.*, 2001), but these have led to diverse pictures about even the qualitative nature of the *P–T* gradients in different sections, and sometimes also in the same section. The latter observation suggests that some of the variations of *P–T* gradients are artifacts of the method of estimation of *P–T* conditions from the mineral chemistry and parageneses. As recently noted by Stephenson *et al.* (2000) and Kohn & Spear (2000), many published *P–T* estimates in the IMS lack enough documentation to convince that appropriate care has been exercised in the choice of mineral compositions that reflect peak metamorphic conditions. Stephenson *et al.* (2000) also noted that many thermobarometric studies of the Himalayan IMS have used rim compositions of phases in mutual contact, and have consequently estimated the diffusion closure conditions, which do not necessarily reflect the peak metamorphic conditions, at least for the high-grade rocks.

We have undertaken a systematic structural and petrological study of the IMS in the Sikkim Himalayas (Neogi *et al.*, 1998; Ganguly *et al.*, 2000), which show the full spectrum of the Barrovian zones. In this work, we report the mineral parageneses within different domains of IMS along a transect in East Sikkim, and estimates of peak metamorphic *P–T* conditions on the basis of detailed thermobarometric calculations

coupled with phase equilibrium constraints, and considerations relating to the kinetic response of mineral compositions to changing *P–T* conditions. Finally, the potential implications of the inferred *P–T* gradient on the models of origin of the Himalayan IMS are discussed. No attempt is made to exhaustively evaluate earlier studies on the determination of *P–T* condition of the Himalayan rocks, nor is it possible to do so without detailed knowledge of the textural relations and the spatial variation of mineral compositions. However, we comment on selected studies and methods to emphasize some of the problems attending the determination of *P–T* condition.

REGIONAL GEOLOGICAL SETTING AND STRUCTURAL HISTORY

Figure 1 shows an overview of the geology of the Himalayas, and location of Sikkim in the eastern Himalayas. Like the other sectors, the Sikkim Himalaya has been subdivided into distinct geotectonic domains, which are separated from one another by thrust faults (Acharya & Shastry, 1979; Ray; 1976; Sinha-Roy, 1982). The Sub-Himalayan domain in the south consists of mollase type deposits of the Siwaliks (Mio-Pliocene), and is separated from the lesser Himalayan domain (LHD) in the north by the Main Boundary Thrust (MBT). Proceeding northwards, the LHD consists of a thin strip of Gondwana rocks (Carboniferous-Permian), carbonate rocks (Buxa Formation) and a thick metasedimentary sequence of dominantly pelites with subordinate psammite and wacke (Daling Group). The overlying higher Himalayan domain (HHD) is composed of medium to high-grade crystalline rocks, commonly referred to as the higher Himalayan crystallines (HHC), which are dominantly of pelitic composition, with sporadic quartzites, calc-silicate rocks, metabasites and small bodies of granite. The HHC is separated from the lesser Himalayas by the Main Central Thrust (MCT). The exact location of this thrust has been controversial in many areas, including Sikkim (Lal *et al*., 1981; Sinha-Roy, 1982). In the far north, a thick pile of fossiliferous Cambrian to Eocene sedimentary rocks belonging to the Tethyan Belt (Tethyan Sedimentary Sequence) overlie the HHC on the hanging wall side of a series of north-dipping normal faults constituting the South Tibetan Detachment System (STDS). The deformation zone related to the MCT is often referred to as the Main Central Thrust Zone (MCTZ). Over the entire length of the Himalayas, the inverted Barrovian sequence is contained essentially within the MCTZ.

Figure 2 shows a regional geological map of Sikkim in the Eastern Himalayas. It has been developed on the basis of mapping conducted by us and available data from other sources (Ray, 1976; Acharya & Shastry, 1979; Sinha-Roy, 1982; Neogi *et al*., 1998). The Rongli transect, in the eastern part of Sikkim, is the focus of the present study. This area was chosen primarily because of the reported presence of a sequence of all

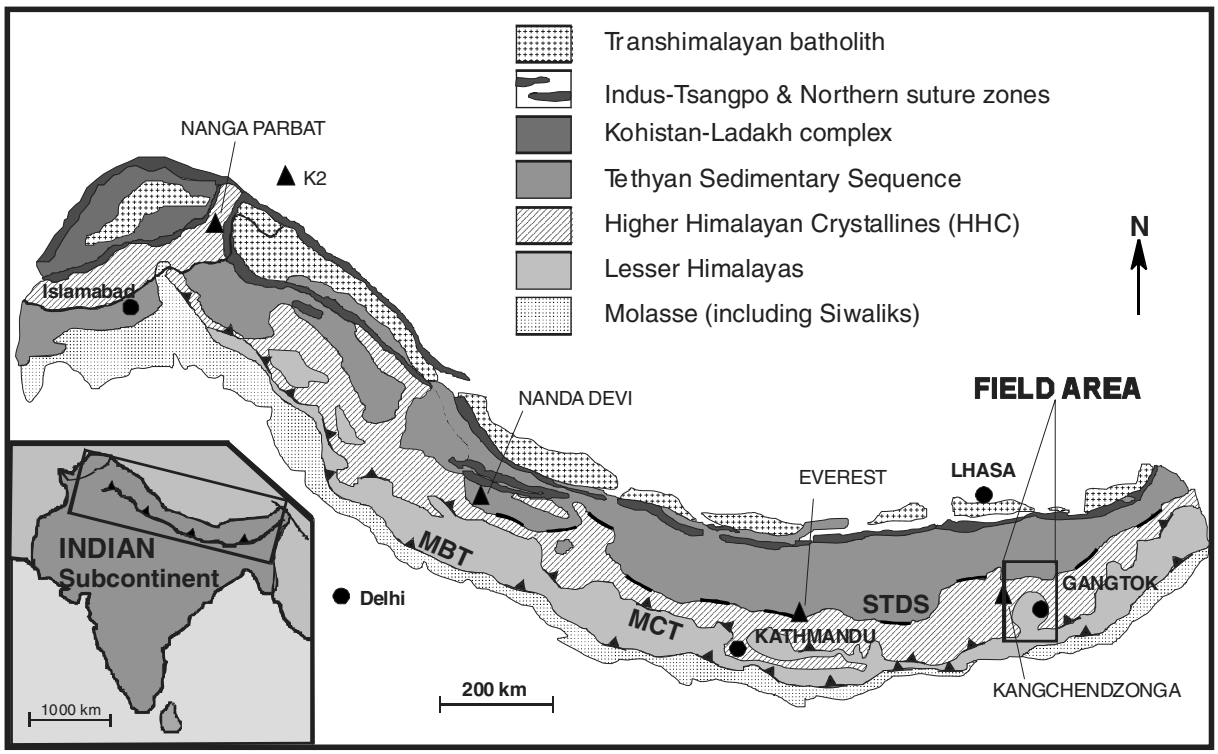

Fig. 1. An overview of some of the major lithological and structural units of the Himalayas, and location of the study area. MBT, Main boundary thrust; MCT, Main central thrust; STDS, South Tibetan detachment system.

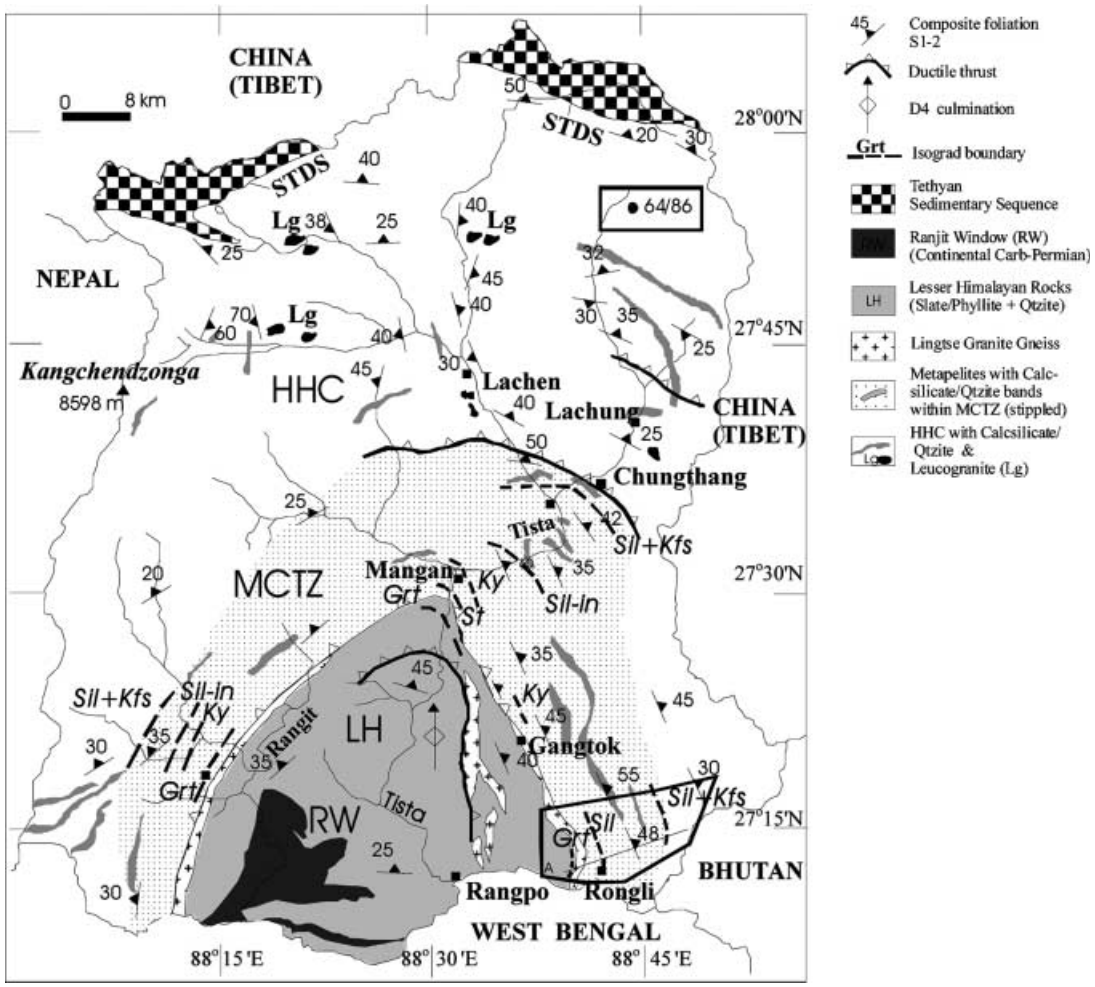

Fig. 2. Simplified geological map of Sikkim showing the known locations of the inverted Barrovian zones, different tectonic domains, foliation attitudes and lithological units. The primary study area is highlighted by a polygon. The kyanite and staurolite isograd boundaries are not shown within the study for the sake of clarity. The stippled area indicates the Main Central Thrust Zone (MCTZ). The sample locations selected for thermobarometric studies are shown in Fig. 3, which is a cross-section approximately along the line within the polygon.

the Barrovian metamorphic zones within a distance of about 20 km. Along this transect, metamorphism progressed in an easterly direction from chloritic, micaceous phyllite and quartzite to different varieties of micaschist, culminating in the appearance of migmatitic pelites. A dominant eastward dipping pervasive planar structure indicates that the whole section is an IMS. A well-foliated granodioritic augen gneiss, locally named as Lingtse Gneiss, is exposed in the middle of the sequence.

The MCTZ in the study area is identified as a large-scale high-strain zone of distributed deformation, as can be determined on the basis of detailed meso- and micro-structural analysis (Neogi *et al.*, 2004). This criterion of the MCTZ in the Sikkim Himalaya is similar to that proposed by Pêcher (1989) in Nepal, Grujic *et al.* (1996) in Bhutan and Stephenson *et al.* (2000) from Zanskar. The MCTZ has variable exposed thickness in Sikkim, and in the present study area it is *c.* 12 km wide, involving both the so-called lesser and higher Himalayan rocks, and extending from the biotite zone to beyond the muscovite-out isograd. Rocks below the MCTZ are referred to as the LHD and those above it as the HHD. Figure 3 shows a schematic E–W cross-section, along the line (approximately E–W) shown in Fig. 2, illustrating the disposition of the isograds, and normally projected locations of the samples that were selected for thermobarometric studies. The foliation and isograd attitudes are extrapolated downwards from surface or near surface measurements. The change of attitudes of shear zones and of foliations near the shear zones have been drawn on the basis of observations in some exposed vertical sections. The arrows indicate the sense of shear.

Three groups of major planar fabrics, S_1, S_2 and S_3 were recognised. The S_1 is an incipient fabric, which is parallel to the compositional layering in the lesser Himalayas, and is commonly preserved as an included

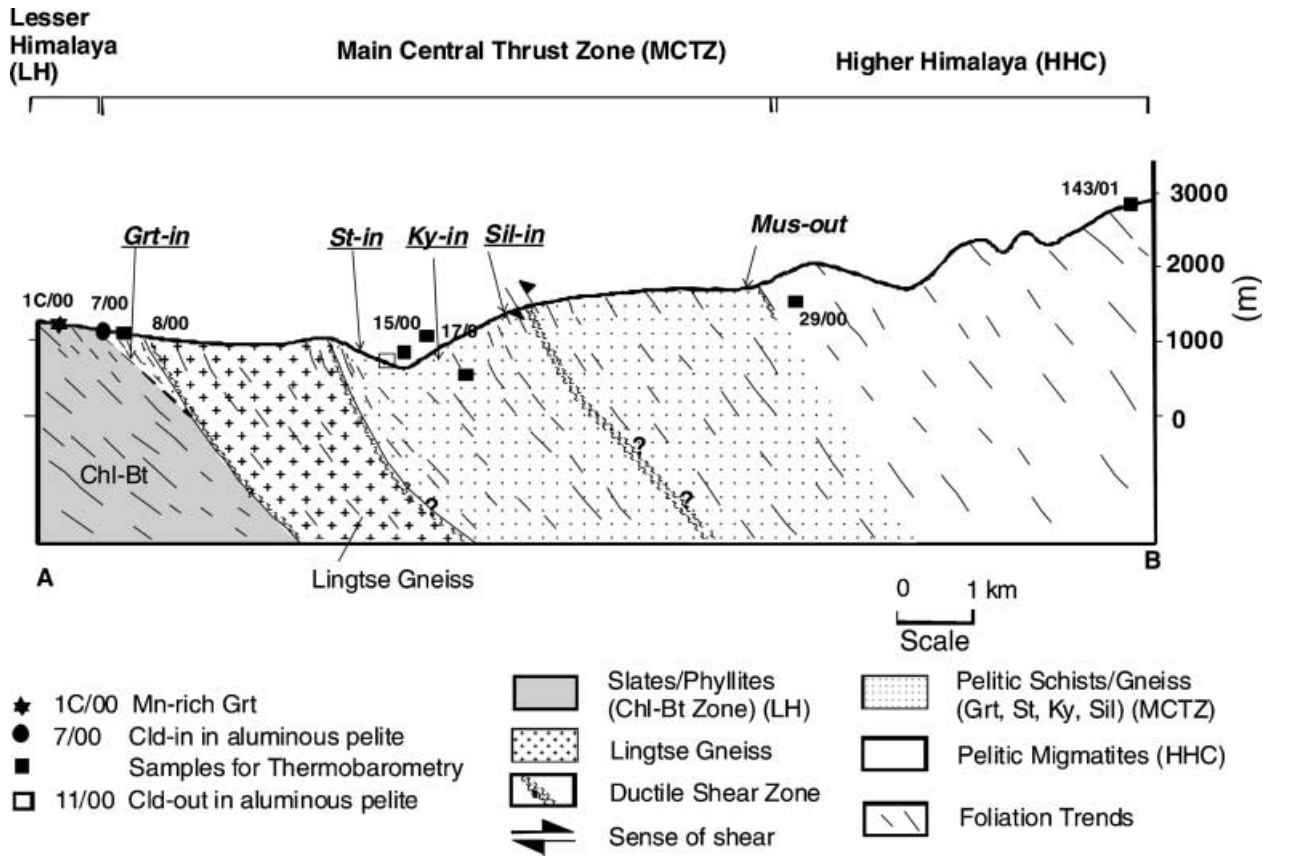

Fig. 3. Schematic cross section along the approximately E–W line in the Rongli transect of eastern Sikkim, shown in Fig. 2, illustrating the disposition of the Barrovian isograds, Lingtse gneiss, and the normally projected locations of the samples used for thermobarometry (filled squares), along with a few additional samples discussed in the text. The horizontal and vertical scales are the same. The foliation and isograd attitudes are extrapolated downwards from surface or from near surface measurements. The change of attitudes of shear zones and of foliations near the shear zones have been drawn on the basis of observations in some exposed vertical sections. The arrows indicate the sense of shear.

fabric in the porphyroblastic phases in the MCTZ (Fig. 4a). The S_2 is the most pervasive planar fabric in all domains, being a slaty cleavage in the chlorite and biotite zones, a schistosity in the garnet to sillimanite-muscovite zones, and a gneissosity in the sillimanite + K-feldspar zone. The orientation of this planar fabric along the transect is roughly the same throughout, that is below, within and above MCTZ (Figs 2 & 3). The S_3 represents a crenulation cleavage or schistosity on S_2 (Fig. 4a). In the higher grade rocks, S_3 is represented by a mylonitic foliation. Also, the metamorphic isograds are roughly parallel to the S_2 planar structures with the higher grade rocks appearing progressively northwards, eastwards (present study area), and westwards of what is known as the Tista Dome (Fig. 2). These observations suggest that a regional deformation folded the metamorphic isograds with approximately a northerly plunge.

Kinematic shear sense was determined at one location in the Rongli transect, which is illustrated in Fig. 3, and at several localities along the Tista river in North Sikkim. In the Rongli location the shear sense is top to SW, whereas in the Tista transect, it is top to S or SSW. The horse-shoe or mushroom shaped pattern of the Darjeeling–Sikkim region, which is attributed to the Tista culmination zone, is due to the interference of E–W and N–S folds (Ray, 2000). Whereas the northerly plunging antiformal structures can be found in Sikkim, the E–W synformal structures are exposed in the Kalimpong and Darjeeling areas, which are located further south of the map area of Fig. 2. The huge arch of the Tista culmination has exposed a vast expanse of the lesser Himalayan units in the core.

PETROGRAPHY

A large number of thin sections have been examined to develop a comprehensive picture of the variation of mineral parageneses, and the relationship between crystallization and deformation in the sequence of metapelites exposed along the Rongli transect. The microstructural relationships have been described in detail in Neogi *et al.* (2004). The crystallization of the index minerals was found to be temporally related to

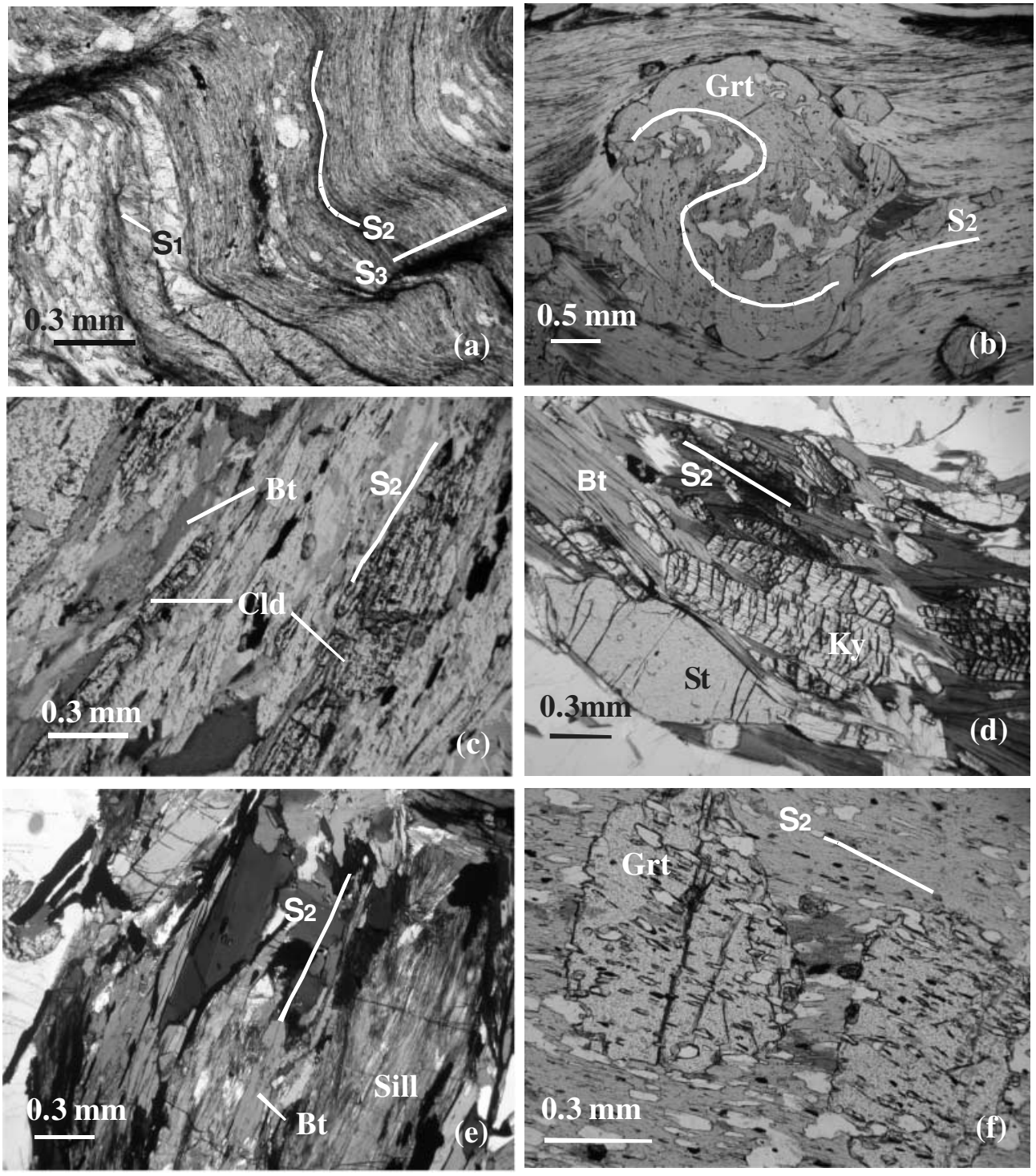

Fig. 4. Photomicrographs (along with sample Nos.) from thin sections showing (a) Quartz (Qtz)-rich microlayers alternating with mica (both muscovite and biotite)-rich layers in a biotite zone pelite with development of the pervasive S_2 schistosity/cleavage, S_3 crenulation cleavage on S_2, and included S_1 streaks (1/99; NE corner of the study area marked in Fig. 2); (b) Snowball garnet with rotation of included S_2 foliation (highlighted by a curved line) in a staurolite grade sample (15/00); (c), (d) and (e): S_2-parallel orientation of prismatic chloritoid (Cld) in a garnet zone aluminous pelite (c: 7/00), staurolite plus kyanite (d: 19/00), and sillimanite (e: CLN8A/03; North Sikkim); (f) garnet crystals with nearly straight inclusion trail merging to the external S_2 foliation; slight rotation of foliation between the two crystals suggest late-tectonic crystallization, possibly extending to post-tectonic (135/01: high-alumina pelite, close to 8/00 in Fig. 3). The locations of the samples 15/00, 7/00 and 19/00 are shown in Fig. 3.

Table 1. Summary of mineral assemblages (plus quartz) in different metamorphic zones along the Rongli transect in East Sikkim.

Pelitic composition	Metamorphic zone	Lesser Himalayan domain	Main Central Thrust zone	Higher Himalayan domain
Sub-aluminous	Chl	Chl, Ms, ±Kfs, Ilm, Mag, Gr		
	Bt	Bt, Chl, Ms, ±Plag, Ilm, ±Allanite ± Tour ± Gr		
Mn-rich	Bt	Grt, Bt, Chl, Ms, Ilm, Gr		
Sub-aluminous	Bt		Bt, Chl, Ms, ±Pl, Ilm, ±Allanite ± Tour ± Gr	
Sub-aluminous	Grt		Grt, Chl, Bt, Ms, Ilm ± Pl ± Gr	
Aluminous	Grt		Cld, Chl, Ms, Bt, Ilm, ±Grt	
Sub-aluminous	St		St, Grt, Bt, Ms, Ilm	
Aluminous	St + Ky		St, Ky, Fibrolite, Grt, Bt, Ms, Pl, Ilm	
Sub-aluminous	Ky		Ky, Grt, ±St, Bt, Ms, Ilm	
Aluminous	Ky		Ky, Bt, Ms, Ilm	
Aluminous	Sil		Sil, ±Ky, Grt, Bt, Ms, Pl, ±Ilm	
+Sub-aluminous	Sil-K-fsp/ Ms-out		Sil, Grt, Bt, Kfs, Ilm, Pl	Sil, Grt, Bt, Kfs, Ilm, Pl

the S_2 fabric in all domains. The mineral growths were primarily syn-S_2, but might have also continued to the post-S_2 phase in some cases. Snowball garnet (Fig. 4b) with rotated trails of relatively fine grained inclusions merging to the dominant S_2 fabric in the matrix, which is devoid of similar pattern of schistosity, and prismatic chloritoid, kyanite, staurolite and sillimanite oriented parallel to the dominant S_2 fabric (Fig. 4c–e) are considered to be unambiguous products of broadly syn-S_2 crystallization. In some cases, the prismatic kyanite grains aligned parallel to the S_2 fabric were also folded along with the latter. There are also garnet (Fig. 4f) and staurolite grains with straight (or nearly so) S_i fabric that is continuous with the external S_2 foliation. The crystallization of these grains was interpreted to be late- to post-S_2. However, Chakraborty *et al*. (2004) have presented an alternative explanation of this texture as syn- or even pre-tectonic on the basis of arguments relating to mass transport and nucleation kinetics.

From the mineral chemistry and modal abundance of the minerals, we identified two major pelitic bulk compositions, *viz*. a sub-aluminous group and an aluminous group. The mineral assemblages in different bulk compositions and metamorphic zones are summarized in Table 1. Unless stated otherwise, the mineral reactions, as written below, simply indicate the major mineralogical changes, and have not been balanced to conserve masses. Mineral abbreviations used are after Kretz (1983).

The LHD: chlorite and part of the biotite zones

In these zones, millimetre to centimetre scale domains of phyllosilicate-rich (muscovite + chlorite) and quartzose bands define a compositional layering (S_0). Muscovite in the chlorite zone is rich in paragonite (≤12 mol.%) and celadonite (≤16 mol.%). The latter was calculated after Holdaway *et al*. (1988), and found to decrease in the biotite zone.

In a rare outcrop within the biotite zone, idiomorphic (50–75 μm) Mn-rich garnet porphyroblasts were observed, which show strong growth zoning with around $Sps_{50}Alm_{34}Prp_3Grs_{13}$ at the core and around $Sps_{20}Alm_{63}Prp_7Grs_{10}$ at the rim. Since Mn fractionates strongly into garnet, the stability limits of garnet are expanded in Mn-rich bulk compositions. These rocks contain significant amount of plagioclase, which shows compositional zoning from around $Ab_{75}An_{25}$ at the core to around $Ab_{84}An_{16}$ at the rim. Garnet presumably formed by the displacement of the reaction

$$\text{Chl} + \text{Qtz} + \text{Pl(An-rich)} \Rightarrow \text{Grt} + \text{Pl(An-poor)} + \text{H}_2\text{O} \quad (1)$$

to lower temperature due to the increased Mn content of the rock.

The MCTZ

The biotite zone rocks occurring in the MCTZ are petrologically similar to those in the LHD (Fig. 2). The other Barrovian zones are briefly described below.

Garnet zone

Garnet in sub-aluminous pelites and chloritoid in aluminous pelites appear simultaneously almost at the beginning of MCTZ. About 500 m down-section from the occurrence of the chloritoid-bearing rock, the aluminous pelite does not contain chloritoid in the matrix, but instead an assemblage of relatively Mn-poor garnet (X_{Mn} around 0.05) + staurolite + kyanite. Sub-aluminous pelites contain Mn-rich garnet (X_{Mn} around 0.17 at the core) and staurolite about 100 m down-dip. Thus, we place the Grt + St + Ky bearing high-alumina pelite in the transition between the garnet and staurolite zones in the sub-aluminous pelites.

Both garnet and chloritoid are present in some thin sections of aluminous pelites, but are segregated in 1–5 mm thick layers, with the garnet having a relatively Mn-rich composition (core composition $Alm_{76}Prp_{03}Sps_{15}Grs_{06}$) and a well-preserved growth zoning. The chloritoid bearing layers are commonly rich in muscovite and have minor chlorite. The formation of chloritoid and garnet in Mn-poor and Mn-rich bands, respectively, is due to the effect of Mn in expanding the field of stability of garnet.

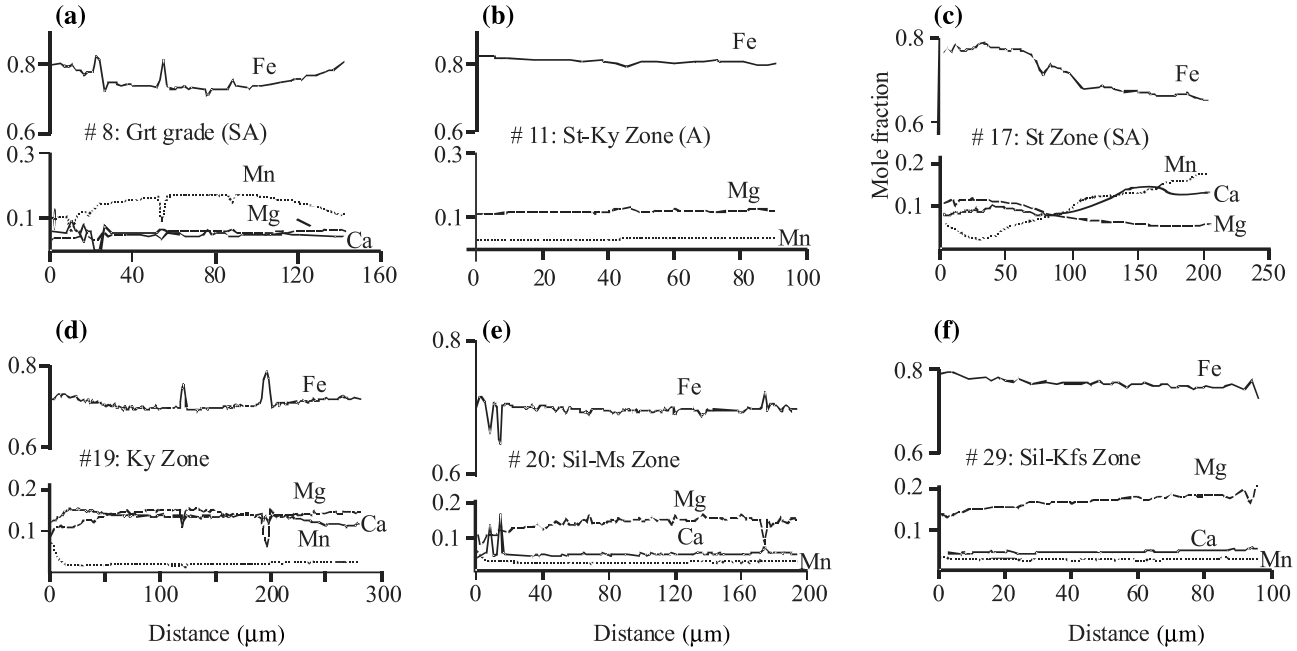

Fig. 5. Compositional zoning in garnet in different zones in the study area along the Rongli transect of eastern Sikkim. The numbers on the panels indicate the sample numbers (omitting the numbers after the slash). The distance is from rim to interior. A, aluminous pelites; SA, sub-aluminous pelites.

Garnet-bearing sub-aluminous pelite

There is a marked decrease in the modal abundance of chlorite, particularly in garnet-bearing domains. Garnet shows preservation of growth zoning (Fig. 5a) with the composition varying from around $Alm_{72}Prp_{05}Grs_{06}Sps_{17}$ in the core to around $Alm_{81}Prp_{05}Grs_{04}Sps_{10}$ near the rim. Biotite in contact with garnet has slightly different compositions from those away from it (contact biotite: $X_{Fe} = 0.49$, $X_{Mg} = 0.29$, $X_{Ti} = 0.05$, $X_{Al(6)} = 0.17$; distant biotite: $X_{Fe} = 0.52$, $X_{Mg} = 0.30$, $X_{Ti} = 0.04$, $X_{Al(6)} = 0.14$). Ilmenite contains 6 mol.% pyrophanite. The compositions of garnet and ilmenite indicate Mn-rich bulk composition. The observed depletion of chlorite in garnet-rich layers suggests that garnet formed from the breakdown of chlorite, such as

$$\text{Chl} + \text{Qtz} \Rightarrow \text{Grt} + \text{H}_2\text{O} \qquad (2)$$

Staurolite-kyanite zone in high-aluminous pelite

The rocks are characterized by the first appearance of staurolite and kyanite. There are minor amounts of retrograde chlorite replacing staurolite and garnet. Garnet is distinctly poor in Mn compared with that of the previous assemblages, and shows considerable relaxation of the growth zoning (Fig. 5b). Biotite shows only minor compositional variation regardless of spatial distribution and grain size. Plagioclase is sodic (X_{An} around 0.2) and shows no zoning even when it is in contact with garnet. The latter observation implies that garnet did not suffer a resorption reaction to produce a plagioclase bearing assemblage in these rocks. Presence of rare chloritoid inclusions in garnet and of staurolite in the same thin section suggest a reaction of the type

$$\text{Cld} + \text{Qtz} \Rightarrow \text{St} + \text{Grt}(\pm\text{Chl}) + \text{H}_2\text{O} \qquad (3)$$

Staurolite zone

This zone is demarked on the basis of the presence of staurolite with relatively Mn-rich garnet. Garnet grains show partly preserved growth zoning, and an increase of Mn content in the rim (Fig. 5c). The modal abundance of garnet is distinctly less than that in similar rocks at lower grades. There is total disappearance of prograde chlorite, whereas biotite is intergrown with staurolite. These observations suggest formation of staurolite plus biotite at the expense of chlorite, for example,

$$\text{Grt} + \text{Chl} + \text{Ms} \Rightarrow \text{St} + \text{Bt} + \text{Qtz} + \text{H}_2\text{O} \qquad (4)$$

Kyanite zone

Two groups of metapelites were recognized in this zone. One group has high-modal abundance of kyanite (> 25% by volume) with very little garnet, while the other is characterized by high-modal garnet and very few kyanite grains. The former possibly represents aluminous and the latter sub-aluminous pelites. Staurolite is present only as rare inclusions in outer massive portions of garnet. The rock is locally migmatitic with quartz plus plagioclase-bearing leucosomes alternating

with biotite-rich melanosome. Garnet shows poorly preserved growth zoning and retrograde diffusion zoning (increase of Fe and Mn and decrease of Mg) near the rim (Fig. 5d) at the contact with biotite. Biotite grains in the matrix do not show any appreciable variation of composition irrespective of whether these are in contact with garnet or not. Plagioclase shows a flat profile with X_{An} around 0.43.

Petrographic features, namely the preservation of rare staurolite inclusions in the outer rims of garnet and presence of kyanite in the same thin section, suggest the reaction

$$St + Qtz \Rightarrow Grt + Ky + H_2O \quad (5)$$

and/or

$$St + Bt + Qtz \Rightarrow Grt + Ky + Ms + H_2O \quad (6)$$

Sillimanite-muscovite zone

In this zone, pelitic rocks contain prismatic sillimanite, and rarely relict kyanite, along with muscovite. K-feldspar is present at places and locally occurs with quartz and plagioclase in the leucosomes. Garnet shows retrograde diffusion zoning of Fe and Mg (Fig. 5e) near the rim, especially when it is in contact with matrix biotite, as expected from the change of equilibrium composition at the interface during exhumation (Ganguly *et al.*, 2000). There is also a small increase of Mn concentration near the rim. Muscovite contains around 14 mol.% paragonite and 0.08 Mg pfu (on 11 oxygen basis), identical to that in the previous zone. Plagioclase is sodic (X_{An} around 0.22) and shows no significant zoning.

HHD: sillimanite + K-feldspar zone

With the total elimination of primary muscovite, K-feldspar appears as a dominant constituent along with garnet, prismatic sillimanite and biotite well within the MCTZ. The pelitic migmatites are by far the most dominant constituent of the HHD in this zone, and consists of Qtz + Kfs (locally perthitic) + minor Pl bearing leucosomes dotted with small euhedral garnet, and mesosomes with porphyroblasts of garnet, biotite and sillimanite. Garnet becomes considerably Mg-rich at this grade and shows well developed retrograde zoning of Fe and Mg near the rim when these are in contact with biotite (Fig. 5f).

GEOTHERMOBAROMETRY

From staurolite through sillimanite zones, the peak metamorphic *P–T* conditions were estimated from garnet–biotite (Grt–Bt) Fe–Mg exchange thermometer and the garnet–aluminosilicate–plagioclase–quartz (GASP) barometer, with careful consideration of the problem of readjustment of mineral compositions during both prograde and retrograde *P–T* variations. The *preferred formulations* of these thermometer and barometer are discussed below. We did not follow the common approach of using a number of published formulations of some specific thermometer(s) and barometer(s), and then showing the average and the spread of the *P–T* solutions. Instead, our own formulations were developed on the basis of well documented experimental data demonstrating attainment of equilibrium in the simple systems, and incorporating the effects of solid solution on the relevant equilibria on the basis of well tested thermodynamic solution properties. The retrieved *P–T* conditions have been compared with additional phase equilibrium constraints to check their reliability. This approach is more robust in terms of addressing the key issue of the *nature* of *P–T* gradient in the IMS, since the *relative* errors in the *P–T* calculations from the same combination of thermometer and barometer, which are based on well constrained experimental and mixing property data, is extremely unlikely to yield a wrong gradient, especially when the results show very good agreement with independent phase equilibrium constraints.

These results of *P–T* calculations are illustrated in Fig. 6 (triangles), along with additional calculations according to the *average P–T method* (squares) of Powell & Holland (1994), which is implemented in their THERMOCALC program using their thermodynamic data base (Holland & Powell, 1998), and has been used widely for the Himalayan rocks. Since the garnet zone sample (No. 8/00) has no aluminium-silicate, the *P–T* condition for this sample were determined on the basis of Grt–Ms–Bt–Pl (GMBP: Alm + Grs + Ms $\leftrightarrow$ 3 An + Ann) barometer of Hoisch (1990) and Grt–Bt thermometry (preferred formulation). Also included in Fig. 6 is the inferred peak *P–T* condition of a sample, 64/86, which was collected from near the STDS (Fig. 2), and discussed in an earlier study (Ganguly *et al.*, 2000). Because of the folded nature of the isograds, it seems quite appropriate to consider the *P–T* condition of this sample as part of the same Barrovian sequence that affected the present study area. The *P–T* results and the related compositional data of the minerals are summarized in Tables 2 and 3, respectively. Table 2 also shows the mineral assemblages in the samples used for *P–T* calculations. The mineral assemblages found in the lesser Himalayan rocks, however, are not suitable for conventional thermobarometric analyses.

Determination and selection of mineral compositions

The mineral compositions were determined by spot analyses with a Cameca SX 50 electron microprobe using 10 nA beam current at an accelerating voltage of 15 kV, using the following standards: synthetic pyrope, grossular, spessartine and diopside for Mg, Ca, Mn and Si, respectively; natural olivine, jadeite, sphene, chromite and feldspar for Fe, Na, Ti, Cr and K, respectively. The inter- and intra-granular compositional variations of garnet, biotite and plagioclase

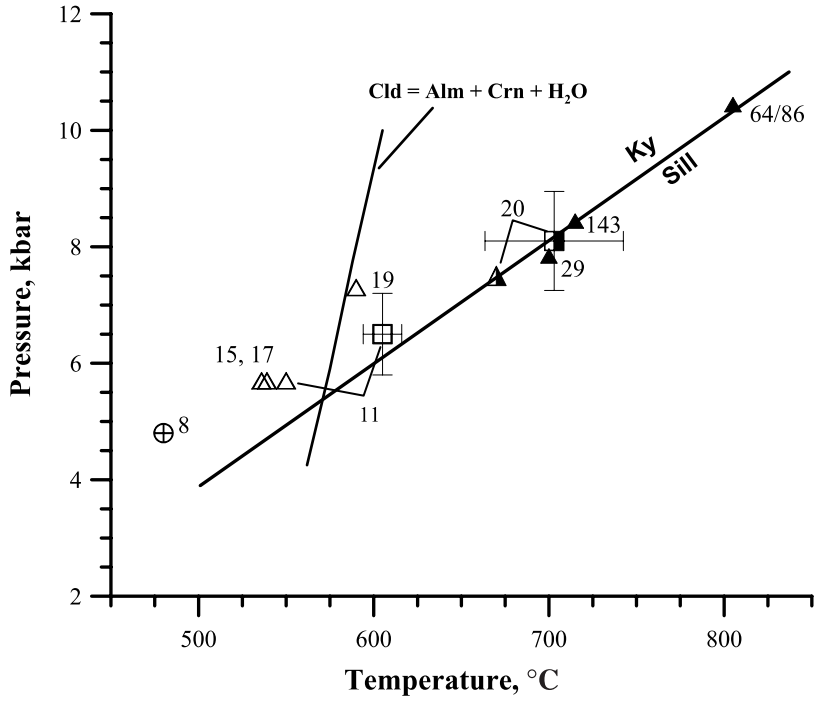

Fig. 6. Calculated *P–T* conditions of rocks from different zones in the inverted metamorphic sequence in eastern Sikkim, India. Triangles, preferred values from simultaneous solutions of Grt–Bt and GASP equilibria. Circle with cross, *P–T* condition according to Grt–Bt (Ganguly formulation) thermometer and GMBP barometer of Hoisch (1990); Square, *P–T* condition according to the average *P–T* method of Powell & Holland (1994). Open and filled symbols indicate the presence of kyanite and sillimanite, respectively, as the only aluminosilicate in the rock, whereas the half-filled symbols indicate the presence of both. Solid line shows the experimentally determined location of the specified equilibrium in the system $FeO–Al_2O_3–SiO_2–H_2O$ (Ganguly, 1969). The numbers besides the symbols indicate the sample numbers (Table 2). The error bars on samples 11 (i.e. 11/00) and 29 (i.e. 29/00) represent $\pm 1\sigma$.

were determined. Biotite grains were found to be homogeneous and also did not show any significant intergranular variation within the scale of a thin section in samples from staurolite and higher grade rocks. Consequently, the choice of biotite grains in these rocks had no significant effect on the temperature estimates. However, small (≤2%) intergranular compositional variations of biotite could be detected within the scale of a thin section in lower grade samples. For the low-grade garnet that preserved growth zoning and did not show any obvious feature related to significant volume diffusion, the rim compositions were paired with the immediately adjacent biotite compositions for the purpose of Grt–Bt thermometry.

Except for samples 15 and 17, the *P–T* conditions of all samples were estimated by simultaneous solutions of the Grt–Bt and GASP equilibria. These two samples do not contain any aluminosilicate. Thus, temperatures were estimated for these samples, using the 'preferred' Grt–Bt exchange thermometer, at pressures determined for the nearest aluminosilicate bearing sample, No. 11, which is within 10–40 m distance. Since the Grt–Bt exchange thermometer is insensitive to errors in pressure estimate (an error of 1 kbar translates to an error of approximately 4 °C), the error introduced by approximating the pressure from samples within a few tens of metres should be insignificant. The following additional points about the choice of mineral compositions should be noted.

(a) In several cases, the compositions of biotite inclusions in garnet, and compositions of garnet at spots which are a few microns away from the inclusions, were used to place a lower limit of peak temperature. (The convolution effect in spot analyses, especially in garnet, become insignificant at around 3 μm distance from an interface (Ganguly *et al.*, 1988)).

Table 2. P–T (kbar - °C) conditions of metapelites from the inverted metamorphic sequence in the Rongli transect, eastern Sikkim.

Sample no. (bulk comp)	Zone	Assemblage	Ganguly	Holdaway/B	Holdaway/M	Holdaway/G	Ganguly Fe(total) = FeO	Method
8/00(SA)	Grt	Grt + Bt + Pl + Qtz + Ms + Chl + Ilm + Gr	4.8–480	5–526	4.9–534	4.9–534	4.9–502	Grt–Bt/GMBP
11/00(A)	St-Ky	Grt + Bt + St + Ky + Ms + Qtz + Chl + Cld + Pl + Ilm	**5.7–550**	5.7–583	5.7–595	5.7–595	6.2–579	Grt–Bt/GASP
17/00(SA)	St	Grt + St + Bt + Ms + Qtz	**5.7–538**	5.7–559	5.7–585	5.7–590	6.2–573	Grt–Bt
15/00(SA)	St	Grt + St + Qtz + Bt + Ms	**5.7–537**	5.7–556	5.7–583	5.7–585	6.2–571	Grt–Bt
19/00	Ky	Grt + Ky + Bt + Qtz + Ms + St (inclusion) + Pl + Ilm	**7.3–590**	7.4–590	7.4–595	7.4–595	7.7–622	Grt–Bt/GASP
20/00	Sil-Ms	Grt + Ms + Bt + Sil + Qtz + Pl + Ilm + Ky (Ky: rare inclusion)	**7.5–670**	7.3–685	7.3–688	7.5–697	7.9–706	Grt–Bt/GASP
29/00	Sil-Kfs	Grt + Bt + Qtz + Sil + Kfs + Pl + Ilm	**7.8–700**	7.9–690	7.9–695	7.8–700	8.1–742	Grt–Bt/GASP
143/01	Sil-Kfs	Grt + Bt + Qtz + Sil + Kfs + Pl + Ilm	**8.4–715**	8.5–795	8.5–796	8.4–800	8.7–755	Grt–Bt/GASP

Ganguly: Grt and Bt solution models from Ganguly *et al.* (1996); Holdaway/B, Holdaway/M and Holdaway/G: Holdaway (2000) formulations with the Berman & Aranovich (1996), modified Mukhopadhyay *et al.* (1997) and Ganguly *et al.* (1996)) garnet solution models, respectively. A represents aluminous; SA represents sub-aluminous and numbers in bold are the preferred values. Pressures for samples 17/00 and 15/00 were assumed to be the same as the adjacent sample 11/00. *P–T* conditions reported in the columns 4–7 are based on an empirical correction for Fe^{3+} content (see text).

Table 3. Selected mineral compositions used in the thermobarometric calculations.

Sample	29 Grt Rim	29 Grt Core	29 Bt Away	29 Bt Contact	29 Pl Core	29 Pl Rim	20 Grt core	20 Grt rim	20 Bt Contact	20 Bt Away	20 Pl Core	20 Pl Rim	20 Ms
Wt%													
SiO_2	38.51	39.12	35.73	35.38	61.86	61.42	38.4	36.63	35.26	34.56	61.64	61.35	46.59
TiO_2	0.08	0.01	2.08	1.95	0.00	0.012	0.01	0.01	2.649	2.29	0.00	0.01	1.09
Al_2O_3	21.02	21.43	19.6	19.37	23.77	23.57	20.4	20.87	18.21	19.02	23.62	23.63	34.25
Cr_2O_3	0.06	0.00	0.01	0.03	0.00	0.00	0.81	0.01	0.00	0.00	0.00	0.02	0.01
FeO	34.04	32.42	18.9	18.58	0.00	0.00	34.26	35.73	20.82	21.34	0.01	0.00	1.38
MnO	1.46	0.96	0.08	0.06	0.00	0.00	0.02	1.05	0.00	0.00	0.06	0.02	0.00
MgO	2.88	4.37	9.11	9.00	0.01	0.00	3.70	3.00	8.69	8.31	0.00	0.00	0.87
CaO	1.25	1.47	0.03	0.03	5.13	5.13	1.35	1.53	0.033	0.00	5.08	5.22	0.04
Na_2O	0.07	0.02	0.26	0.25	8.56	8.77	0.08	0.06	0.43	0.33	8.54	8.56	1.10
K_2O	0.06	0.02	9.37	9.27	0.38	0.23	0.02	0.01	8.40	8.41	0.15	0.16	9.30
Total	99.44	99.83	95.18	93.94	99.71	99.13	99.06	98.91	94.49	94.27	99.1	98.97	94.64
Cations													
Si	2.96	3.10	5.30	5.31	2.752	2.75	3.09	2.99	5.43	5.23	2.78	2.75	6.22
Ti	0.00	0.00	0.23	0.22	0.00	0.00	0.00	0.00	0.31	0.29	0.00	0.00	0.11
Al	2.08	2.00	3.43	3.43	1.25	1.24	1.94	2.00	3.57	3.39	1.24	1.25	5.38
Cr	0.00	0.00	0.00	0.00	0.00	0.00	0.06	0.00	0.00	0.00	0.00	0.00	0.00
Fe	2.29	2.15	2.14	2.13	0.00	0.00	2.31	2.44	2.48	2.50	0.00	0.00	0.15
Mn	0.10	0.06	0.01	0.01	0.00	0.00	0.00	0.07	0.00	0.00	0.00	0.00	0.00
Mg	0.35	0.52	2.01	2.02	0.00	0.00	0.44	0.36	1.99	1.97	0.00	0.00	0.17
Ca	0.11	0.12	0.00	0.00	0.24	0.24	0.12	0.13	0.00	0.00	0.22	0.22	0.01
Na	0.00	0.00	0.07	0.07	0.74	0.76	0.01	0.01	0.13	0.10	0.77	0.77	0.28
K	0.01	0.00	1.77	1.78	0.02	0.01	0.00	0.00	1.65	1.62	0.01	0.01	1.58
Total	7.90	7.95	15.17	15.17	5.00	5.01	7.97	8.01	15.56	15.10	5.02	5.00	13.90

Sample	19 Grt Core	19 Grt Rim	19 Bt Contact	19 Bt Away	19 Pl Core	19 Pl Rim	19 Ms	17 Grt Rim	17 Bt Contact	15 Grt Rim	15 Bt Contact	143/01 Grt Core	143/01 Bt Away	143/01 Pl Core
Wt%														
SiO_2	37.22	37.91	36.53	37.78	57.45	56.91	45.57	36.06	36.01	36.09	36.47	36.13	35.12	63.71
TiO_2	0.01	0.02	1.23	1.11	0.02	0.02	0.27	0.16	1.31	0.10	1.59	0.02	1.96	0.00
Al_2O_3	21.41	21.63	18.59	20.7	27.01	26.96	36.09	20.6	18.91	20.41	19.49	20.98	18.54	21.95
Cr_2O_3	0.00	0.00	0.08	0.04	0.00	0.03	0.00	0.07	0.07	0.00	0.00	0.02	0.04	0.00
FeO	32.79	32.21	17.39	16.97	0.03	0.03	1.75	34.58	18.19	34.15	17.4	28.06	17.86	0.15
MnO	0.92	0.62	0.00	0.00	0.01	0.00	0.00	1.18	0.10	1.07	0.00	8.94	0.42	0.00
MgO	3.71	3.81	11.32	11.93	0.01	0.00	0.49	2.94	10.52	2.9	10.84	4.54	10.43	0.00
CaO	3.92	4.38	0.11	0.19	8.89	8.70	0.00	2.88	0.01	3.04	0.01	0.87	0.00	2.87
Na_2O	0.05	0.02	0.18	0.23	6.71	6.90	1.49	0.05	0.46	0.07	0.17	0.00	0.14	9.83
K_2O	0.00	0.02	8.50	7.37	0.07	0.09	8.78	0.01	8.62	0.00	7.90	0.00	9.74	0.33
Total	100.05	100.61	93.93	96.33	100.21	99.64	94.43	98.54	94.21	97.83	94.04	99.54	94.23	98.83
Cations														
Si	2.97	2.99	5.42	5.41	2.63	2.62	6.09	2.95	5.35	2.97	5.4	2.91	5.39	2.85
Ti	0.00	0.00	0.14	0.12	0.00	0.00	0.03	0.01	0.01	0.01	0.18	0.00	0.23	0.00
Al	2.01	2.01	3.25	3.49	1.46	1.47	5.67	1.99	3.31	1.98	3.40	1.99	3.34	1.16
Cr	0.00	0.00	0.01	0.00	0.00	0.00	0.00	0.00	0.01	0.00	0.00	0.00	0.01	0.00
Fe	2.19	2.13	2.16	2.03	0.00	0.00	0.20	2.37	2.26	2.35	2.15	1.89	2.29	0.00
Mn	0.06	0.04	0.00	0.00	0.00	0.00	0.00	0.08	0.15	0.07	0.00	0.61	0.05	0.00
Mg	0.44	0.45	2.50	2.55	0.00	0.00	0.10	0.36	2.33	0.36	2.39	0.55	2.39	0.00
Ca	0.30	0.37	0.02	0.03	0.44	0.43	0.00	0.25	0.00	0.27	0.00	0.08	0.0.	0.14
Na	0.01	0.00	0.05	0.07	0.56	0.57	0.39	0.01	0.14	0.01	0.05	0.00	0.04	0.85
K	0.00	0.00	1.61	1.35	0.00	0.01	1.50	0.00	1.64	0.00	1.49	0.00	1.91	0.02
Total	7.98	8.00	15.15	15.05	5.10	5.10	13.96	8.02	15.20	8.01	15.06	8.03	15.64	5.01

Sample	Grt 11 Rim	Grt 11 Incl	Bt 11 Contact	Bt 11 Incl	Pl 11 Core	Pl 11 Rim	Ms 11	Grt 8 Rim	Bt 8 Contact	Pl 8 Rim	Ms 8
Wt%											
SiO_2	36.17	36.71	35.32	34.94	63.35	63.35	46.65	36.39	35.17	66.59	45.44
TiO_2	0.00	0.01	1.53	1.49	0.00	0.00	0.24	0.00	1.91	0.02	0.19
Al_2O_3	20.75	20.86	18.93	18.96	23.63	23.35	36.25	20.87	18.86	21.93	35.87
Cr_2O_3	0.04	0.00	0.00	0.00	0.01	0.01	0.00	0.02	0.00	0.00	0.00
FeO	36.51	35.83	20.48	21.44	0.00	0.02	1.46	35.42	23.72	0.01	1.54
MnO	1.33	1.35	0.07	0.00	0.04	0.00	0.01	4.25	0.15	0.00	0.00
MgO	2.7	2.85	9.20	8.40	0.00	0.00	0.57	1.38	7.56	0.00	0.64
CaO	1.41	1.48	0.00	0.00	4.32	4.17	0.00	1.35	0.00	1.87	0.00
Na_2O	0.01	0.02	0.44	0.24	9.38	8.71	1.55	0.05	0.08	10.56	1.09
K_2O	0.02	0.01	9.05	9.89	0.09	0.10	8.59	0.00	8.23	0.05	9.52
Total	98.94	99.13	95.02	95.37	100.84	99.71	95.31	99.73	95.67	101.03	94.29

Table 3. (*Cont'd*).

Sample	Grt 11 Rim	Grt 11 Incl	Bt 11 Contact	Bt 11 Incl	Pl 11 Core	Pl 11 Rim	Ms 11	Grt 8 Rim	Bt 8 Contact	Pl 8 Rim	Ms 8
Cations											
Si	2.96	2.99	5.41	5.38	2.85	2.88	6.15	2.98	5.41	2.89	6.09
Ti	0.00	0.00	0.16	0.00	0.00	0.00	0.02	0.00	0.22	0.00	0.02
Al	2.00	2.00	3.50	3.42	1.25	1.25	5.62	2.01	3.41	1.12	5.60
Cr	0.00	0.00	0.00	0.00	0.00	0.00	0.00	0.00	0.00	0.00	0.00
Fe	2.50	2.44	2.66	2.76	0.00	0.00	0.16	2.42	3.05	0.00	0.17
Mn	0.09	0.09	0.01	0.00	0.00	0.00	0.00	0.29	0.02	0.00	0.00
Mg	0.33	0.35	2.10	1.92	0.00	0.00	0.11	0.17	1.73	0.00	0.13
Ca	0.12	0.13	0.00	0.00	0.21	0.20	0.00	0.12	0.00	0.10	0.00
Na	0.00	0.00	0.13	0.07	0.82	0.77	0.40	0.01	0.03	0.90	0.28
K	0.00	0.00	1.76	1.94	0.01	0.01	1.45	0.00	1.61	0.01	1.63
Total	8.02	8.01	15.84	15.49	5.13	5.11	13.91	8.01	15.48	5.02	13.93

The cation proportions in garnet, mica and plagioclase are on 12, 22 and 8 oxygen basis, respectively.
Contact, in contact with garnet; Away, removed from garnet; Incl, included in garnet.

(b) For high-grade garnet that shows flat core compositions and retrograde zoning near the rim (Fig. 5e–f), the peak P–T conditions were computed using core compositions of garnet of at least 1.5 mm radius. The choice of grain size is based on the analysis of Ganguly & Tirone (1999), who showed that core compositions of garnet surrounded by a very rapidly diffusing matrix, such as biotite, would not be significantly affected during cooling if the peak temperature (T_o) did not exceed 900 °C and the value of a dimensionless parameter, M, is ≤0.1. This parameter incorporates the effects of grain size, cooling rate and diffusion kinetics on the resetting of composition. It is defined as

$$M = \frac{RD(T_o)T^2}{E(dT/dr)r^2}$$

where R is the gas constant, $D(T_o)$ is the Fe–Mg interdiffusion coefficient at T_o, E is the activation energy of diffusion, dT/dt is the cooling rate at the temperature T, and r is the radius of a garnet grain of spherical geometry.

Ganguly *et al.* (2000) determined the exhumation and cooling rate of a sillimanite + K-feldspar grade rock (No. 64/86) from North Sikkim. They deduced a two stage exhumation process, an initial nearly isothermal (at about 800 °C) exhumation from around 34 km to around 11 km depth, followed by much slower exhumation of approximately 2 mm year^{-1}. (Since the exhumation velocity was held constant, the cooling rate associated with the second stage was variable, starting at around 25 °C Myr^{-1} at 800 °C and increasing smoothly to around 300 °C Myr^{-1} near the surface.) Using $T_o = 800$ °C, dT/dt at T_o of 25 °C Myr^{-1} and the Fe–Mg diffusion parameters from Ganguly *et al.* (1988), yield $r = 0.6$ mm. Reducing the cooling rate by a factor of 5 increases r by the factor of $\sqrt{5}$, that is to 1.3 mm. In other words, if the initial cooling rate of the rock was ≥5 °C Myr^{-1}, then the core compositions of garnet grains of at least 1.3 mm radius would not have been affected during cooling from a peak temperature of 800 °C.

(c) For calculation of GASP equilibrium, only those garnet grains in immediate contact with plagioclase were chosen. In some thin sections from both low- and high-grade rocks, a nearly threefold increase in grossular content in garnet was observed, when it is removed from plagioclase. Pressure was computed using matrix-plagioclase in contact with garnet and also plagioclase included in garnet, whenever possible, but no significant difference was found between the two sets of results.

(d) Plagioclase grains did not show any appreciable compositional variation from core to rim (Fig. 7). Thus, an average of 20 spot analyses were used for the plagioclase grains selected for thermobarometric calculations.

(e) The staurolite/kyanite grade rocks show increase of Mn content of garnet grains near the rims

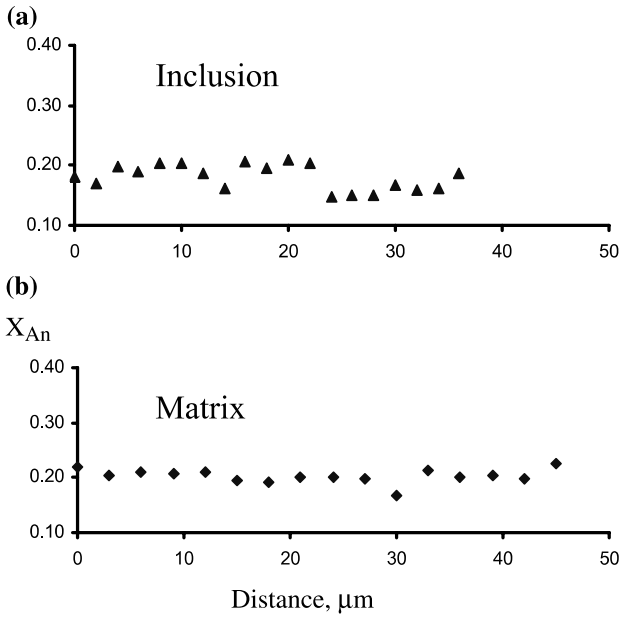

Fig. 7. Compositional profiles in plagioclase (a) included in garnet and (b) in the adjacent matrix (MCT Zone, kyanite grade; Sample no. 19/00, Fig. 3).

(Fig. 5c–d). Qualitatively similar *Mn kick-up* near the rim of garnet has been observed by several workers in medium grade rocks in which the diffusion was not sufficiently effective to completely homogenize the garnet composition at the peak metamorphic condition. Because of the initial bell-shaped profile of Mn, a minimum in the Mn-zoning profile is typically observed near the rim (Fig. 5c). Conventionally, the composition of garnet at the Mn minimum has been paired with adjacent biotite composition to closely approximate the peak metamorphic *P–T* condition. The rationale behind this approach is that the composition of garnet at the Mn minimum represents a close approximation of its rim composition at the peak metamorphic condition, and that the adjacent biotite composition has not significantly changed during cooling. However, for some Himalayan samples from Nepal, Kohn & Spear (2000) found that this approach yields temperatures that are too high compared with that suggested by the mineralogy of the samples. Thus, they suggested that the Mn kick-up near the garnet rims was due to retrograde net transfer (ReNTR) reactions, which increased the Fe/(Fe + Mg) ratio of the adjacent biotite, leading to an increase in the estimated temperatures.

In the studied samples, pairing of garnet composition at the Mn minimum with adjacent biotite did not yield temperatures that might be considered anomalous on the basis of geological and/or petrographic criteria. As noted above, we did not find any significant difference between the compositions of biotite adjacent to, and distant from garnet in these samples. Furthermore, the near rim Mn kick-up of garnet was observed in both plagioclase-bearing and -free samples. Since plagioclase is a product plagioclase in the ReNTRs of garnet (e.g. Grt + Ms $\rightarrow$ Pl + Bt and Grt + Al_2SiO_5 + Qtz $\rightarrow$ Pl), the near-rim Mn kick-up of garnet in the plagioclase-free samples could not have been due to ReNTR. Furthermore, determination of compositions of plagioclase did not show any significant variation either within or between individual grains. Also there is no significant compositional difference between plagioclase grains included in garnet and in the matrix (Fig. 7). These observations rule out formation of plagioclase by ReNTR of garnet.

Mn-kick up near garnet rims may also result from the breakdown of Mn bearing ilmenite (E. Ghent, pers. comm.) Although ilmenite is present in our samples, there is no textural evidence suggesting its breakdown. Thus, for the rocks showing Mn kick-up near garnet rims that were used for thermo-barometric calculations, the most reasonable explanation seems to be the retrograde exchange with biotite. This process must lead to an increase of Mn content of garnet during cooling if the mass of biotite was sufficiently large compared to the exchanging volume of garnet, as the petrographic observations suggest to be the case for the specific samples.

Thermobarometric formulations

Grt–Bt exchange thermometer and GASP barometer

The Grt–Bt exchange thermometer and GASP barometer, which yielded the *P–T* data listed under the two 'Ganguly' columns in Table 2, were formulated, according to well established thermodynamic methods (e.g. Ganguly & Saxena, 1987), using the following data (computer programs for these calculations are available from J.G.). For the exchange thermometer, we used the experimental data of Ferry & Spear (1978) in the Fe–Mg binary system, the multicomponent subregular garnet solution model of Ganguly *et al.* (1996; Table 4), and a mutually compatible biotite solution model therein that was found to satisfactorily account for the compositional dependence of the Fe–Mg distribution coefficient, K_D, of natural samples. Biotite was assumed to follow a regular solution behaviour. The interaction parameters for biotite relevant for Grt–Bt thermometry are as follows. $W_{Fe-Mg} = 0$, $(W_{Mg-Fe3+} - W_{Fe-Fe3+}) = 0$; $(W_{Mg-Ti} - W_{Fe-Ti}) = 10$; and $(W_{Mg-Al} - W_{Fe-Al}) = -2.7$ kJ cation-mol^{-1}. These parameters are from Ganguly *et al.* (1996) that also incorporated the data from Patiño Douce *et al.* (1993).

The GASP barometer was formulated according to the experimental data of Koziol & Newton (1989) for the end-member reaction, garnet solution model of Ganguly *et al.* (1996) and plagioclase solution model of Fuhrman & Lindsley (1988). The garnet solution model of Ganguly *et al.* (1996) is preferred since it is based on the optimisation analysis of much larger set of well-constrained experimental data, extending to Mn-rich samples (Wood *et al.*, 1994; Ganguly *et al.*, 1996), than those used in the earlier models, along with natural data on Mn-rich samples. The choice of the plagioclase solution model was based on the evaluation of Applegate & Hodges (1994). We did not analyse for the Fe^{3+} in garnet and biotite, and carried out the thermobarometric calculations in two different ways: (a) assuming that all iron is divalent, and (b) assuming, in accordance with the average values for the regionally metamorphosed metapelites suggested by Holdaway (2000), that 3 mol.% of total iron in garnet and 11.6 mol.% of that in biotite were in Fe^{3+} state.

For the sake of clarity of illustration, the results obtained from assuming Fe^{2+} = Fe(total) were not plotted. The latter yields *P–T* solutions which are 0.03 ± 0.02 kbar higher and 33 ± 10 °C higher than those calculated using the empirical Fe^{3+} correction (Table 2). However, general trends of *P–T* variation are quite similar in both methods of calculations showing that *both* peak metamorphic temperature and pressure (at the peak temperature) increased progressively towards the foreland (i.e. up section). The *P–T* conditions calculated by using the empirical Fe^{3+} correction and the Grt–Bt and GASP formulations discussed above will be referred to as the *preferred*

values. These are indicated by bold numbers in Table 2.

The Grt–Bt thermometric formulations of Holdaway (2000) were used that permit calculation of temperature using one of the three garnet solution models, *viz*. Berman & Aranovich (1996); Ganguly *et al*. (1996) and Mukhopadhyay *et al*. (1997). Holdaway (2000) modified the last two garnet models to incorporate the Mn-interaction parameters from Ganguly *et al*. (1996), which led to significant improvement of the statistical quality of the temperature calculations of natural assemblages. However, it should be noted that with this modification, there is no significant difference among the three formulations for common pelitic compositions. The Holdaway formulations, which calculate default values of Fe^{3+} contents in garnet and biotite in the same way as stated above (assumption (b)), were used along with the preferred GASP formulation to solve simultaneously for P and T (Table 2).

Phase equilibria and observational constraints

An obvious constraint on the P–T estimates of the rocks is provided by the kyanite–sillimanite boundary, for which the widely used calibration of Holdaway (1971) was used. The results based on the preferred formulations, regardless of whether or not Fe^{2+} was assumed to be equal to Fe(total), are in excellent agreement with the Holdaway calibration in that the estimated P–T condition of an assemblage is completely compatible with the constraint imposed by the nature of the aluminium-silicate polymorph(s) in the assemblage (Fig. 6).

A garnet crystal in the sample 11 was found to contain an inclusion of chloritoid. As discussed below, the solution of the peak P–T condition of this rock must lie below the absolute upper stability of chloritoid, as defined by the reaction (7). Since this sample also contains staurolite in the matrix, it seems likely that peak temperature of this rock was even lower, and was constrained by the equilibrium condition of the reaction Cld + Qtz to St + Grt + H_2O. The stability limits of chloritoid ± quartz were determined by Ganguly (1969) using pure Fe-end members of the solid solution phases. These reactions are

$$3\mathrm{Cld} = \mathrm{Grt} + 2\mathrm{Crn} + 3\mathrm{H_2O} \qquad (7)$$

and

$$23\mathrm{Cld} + \mathrm{Qtz} = 4\mathrm{St} + 5\mathrm{Grt} + 21\mathrm{H_2O} \qquad (8)$$

The equilibrium (7) is shown in Fig. 6. The equilibrium P–T condition of (8), using Fe-end member phases, is about 12 °C lower than that of (7) (Ganguly, 1969). The displacements of these equilibria due to compositional change of the minerals can be calculated from thermodynamic principles (e.g. Ganguly & Saxena, 1987; Eqn 4.33). Assuming ideal ionic solution behaviour, the results show that the equilibria (7) and (8) would be shifted by ≤5 °C due to the solid solution effect in the sample no. 11. The P–T condition of sample 11, as calculated according to the preferred formulations and the empirical Fe^{3+} correction, as discussed above, is consistent with the phase equilibria constraints. Without Fe^{3+} correction, the estimated P–T condition falls right on the equilibrium (7), which suggests that the temperature is somewhat overestimated by this method.

Garnet in samples 15 and 17 are relatively rich in Mn ($X_{Mn} = 0.12$–0.17). These samples are only about 100 m distant from sample 11, in which the Mn content of garnet is much lower. Thus, from the field relations, samples 11, 15 and 17 are expected to have formed at nearly the same P–T condition. This expectation is very closely satisfied by the P–T estimates based on the preferred formulations. The Holdaway (2000) formulations of the Grt–Bt geothermometer yield temperatures for sample 11, which has chloritoid inclusion in garnet, that are 8–20 °C higher than the equilibrium (7) at $X(H_2O) = 1$. There can be no metastable overstepping of chloritoid beyond its *absolute* stability limit within a geological time scale, even if it were included in garnet, since equilibrium (7) was tightly reversed in the laboratory (Ganguly, 1969). Inclusion in garnet or any other phase could not have prevented the thermal breakdown of a mineral if it were not required to react with a matrix phase. Except for one sample (#29), the three garnet mixing models in the Holdaway formulation (Holdaway, 2000) yield somewhat higher temperatures (5–36 °C) than the preferred values. However, for any specific sample, all three garnet mixing models in the Holdaway formulation yield temperatures that differ very little (within ±10 °C, Table 2), as should be expected since, with Holdaway's modifications, all garnet mixing models reduce essentially to that of Ganguly *et al*. (1996) for the observed range of compositions.

The uncertainty of the P–T estimates were not evaluated according to the preferred method. A realistic analysis of this problem is difficult since we have utilized optimised thermodynamic mixing properties. However, the very good agreement of the P–T estimates with independent phase equilibria constraints should ensure the validity of the general trend of the P–T gradient, especially because of the use of the same set of well-calibrated thermobarometers for all samples.

Average *P–T* method

In this method, the P–T condition of a metamorphic rock is determined on the basis of convergence of various equilibria within an observed mineral assemblage (Powell & Holland, 1994; Holland & Powell, 1998). The use of multiple equilibria for calculating P–T conditions would be a preferable practice if the

different equilibria were well constrained by experimental and/or thermodynamic data in the simple systems, and the thermodynamic mixing properties of the mineral solid solutions, which often involve multi-site and multi-component substitutions, were well known. Unfortunately, there is considerable gap between this requirement and the current status of our knowledge in the field. Additionally, if devolatilization equilibria are used in the calculation of *P–T* condition, then it is necessary to have *a priori* knowledge of the fluid composition.

There is no independent constraint on fluid composition in the samples studied in this work. In fact, knowledge of the *P–T* condition is a pre-requisite for the calculation of fluid composition. The absence of any evidence of CO_2 rich fluid cannot be a justifiable rationale for assuming $X(H_2O) = 1$ (e.g. Stephenson *et al.*, 2000). Even in the C–O–H system that may be geologically too simple, there are other volatile species, especially CH_4, which could be present in significant proportion in metapelites that had graphite, even if it had become consumed at the high grade (e.g. Ganguly, 1977). It should also be obvious from the above discussion of bulk and mineral compositional variation that overall equilibrium was not achieved among the minerals within the scale of a thin section in many cases. Simultaneous attainment of equilibrium for the different reactions is an inherent requirement behind the application of the average *P–T* method that needs to be tested for the samples to which this method is applied.

Since the average *P–T* method has been used widely for the Himalayan rocks, several calculations were undertaken according to this method using the program THERMOCALC and its embedded thermodynamic properties for the end members and solutions (Holland & Powell, 1998). When restricted to use only anhydrous equilibria, the average *P–T* method yielded solutions that had too large uncertainties (1σ values: 1.5–1.9 kbar and 80–130 °C) of the estimated *P–T* conditions to be useful in the determination of the *P–T* gradient. For one sample, No. 20, the program used only anhydrous equilibria regardless of whether water was included as a component or not. The *P–T* solution for this sample, 8.1 ± 1.7 kbar, 703 ± 79 °C, is consistent with the result from the preferred formulation (Fig. 6). Sample no. 20 contains sillimanite and rare kyanite grains as relicts within sillimanite. The presence of kyanite could have escaped attention without very detailed petrographic observation. Without kyanite in the input set, the average *P–T* method yielded 8.3(±1.9) kbar, 758(±132) °C, which have too large error bars to be meaningful, and the mean conditions of which significantly violate the kyanite–sillimanite boundary. It seems, therefore, that for aluminium-silicate bearing assemblages, the average *P–T* method constrains the solution to satisfy the equilibrium condition of the aluminosilicate(s), and might yield a significantly erroneous answer if a quantitatively very minor aluminosilicate phase is not identified and introduced in the input data set.

For sample 11, which has the chloritoid inclusion in garnet, the average *P–T* method yielded tightly constrained *P–T* solution of 6.5(±0.7) kbar and 605(±11) °C at $X(H_2O) = 1.0$. However, this is about 20 °C higher than the *absolute* stability limit of chloritoid (Fig. 6). In doing this calculation, chloritoid was not input as a mineral in the computer program, since it is present as an inclusion in garnet, and, therefore, was highly unlikely to have been in equilibrium with the matrix phases. Use of only anhydrous equilibria for this sample yielded a poorly constrained solution of 5.9 ± 1.4 kbar, 601 ± 88 °C.

From the analyses presented above, we conclude that the average *P–T* method is not suitable for the determination of a *P–T* gradient of the samples investigated in this study, and that the requirements for the useful application of this method to natural samples may be difficult to satisfy in many cases. We also note incidentally that Stephenson *et al.* (2000) found that the temperatures obtained from the average *P–T* method, which they preferred, are consistently higher by approximately 100 °C than those obtained from the Grt–Bt thermometric formulation. Part of this disagreement is most likely due to the fact that temperatures were overestimated as a result of the assumption of pure H_2O fluid, and also the fact that the chosen Grt–Bt thermometric formulation (Bhattacharya *et al.*, 1992) is not completely compatible with the subsequent advancement of knowledge of garnet and biotite solution properties (e.g. Ganguly *et al.*, 1996; Holdaway, 2000).

DISCUSSION

A number of models have been proposed to explain the inversion of the Barrovian metamorphic zones in the Himalayas (for reviews, see Hodges, 2000; Vannay & Grasemann, 2001). Very broadly, the existing models can be classified into four groups: (a) thermal inversion models (e.g. Frank *et al.*, 1975; LeFort, 1975; Bhattacharya & Das, 1983; England *et al.*, 1992) that invoke inversion of the metamorphic sequence through transient inversion of isotherms at the level of MCT by placing a hot thrust slice on top of a colder footwall rock, by frictional heating during thrusting, etc; (b) late- to post-metamorphic deformation of the isograds by recumbent folding (e.g. Searle *et al.*, 1999); (c) different schemes of tectonic imbrications along thrusts (e.g. Treloar *et al.*, 1989; Swapp & Hollister, 1991; Robinson *et al.*, 2003); and (d) coupled thermal and tectonic processes in which the inversion of the metamorphic process is considered to be a consequence of syn- to late-metamorphic ductile extrusion (e.g. Jain & Manickavasagam, 1993; Grujic *et al.*, 1996; Hubbard, 1996; Jamieson *et al.*, 1996, 2002; Beaumont *et al.*, 2001; Vannay & Grasemann, 2001).

There are three key observations from our study that contribute to an evaluation of the above models. (a) We find a progressive increase of both temperature and pressure with increasing grade and structural height through the MCTZ and the lower part of the HHC; the *P–T* condition of a sample (64/86) from near the STDS (Figs 2,6) also conforms to the general trend; (b) The growth of metamorphic minerals at all grades is closely related temporally to one dominant planar fabric, S_2; the crystallization is dominantly syn-S_2; (c) There is nothing out of sequence in the studied section, in terms of not only increasing *P* and *T*, but also key mineral parageneses. Also there is no indication of polymetamorphic history in the zoning profiles of garnet, including sample 64/86 which reflects the highest *P–T* condition, and was collected close to STDS. If a granulite grade garnet that shows homogeneous composition at the core, such as in this sample and other sillimanite grade garnet analyzed in this study (Fig. 4), were subjected to two metamorphic episodes, M1 and M2, then the near-rim compositions of garnet would be expected to show oscillation reflecting cooling following M1, heating during M2 and subsequent cooling. No such feature was observed in any high-grade garnet. As shown elsewhere (Ganguly *et al.*, 2000), the zoning profile of the garnet in sample 64/86 can be modelled very well by assuming monotonic cooling from a peak temperature of around 800 °C that is constrained by geothermometry.

An inevitable consequence of the models under group (a) is that increasing temperature up section must be associated with decreasing pressure. Our thermobarometric results clearly contradict these models. Also our observation on the temporal relation between metamorphic crystallization and the most pervasive planar fabric, S_2, which are subparallel in different domains and also to the isograd boundaries, make post-/late-metamorphic inversion of the Barrovian zones by recumbent folding or thrusting to be highly unlikely, even though these models lead to increase of both pressure and temperature with increasing structural heights in the IMS, as observed. Furthermore, as noted by Vannay & Grasemann (2001), large scale recumbent folds have been identified only in a few sections of the Himalayas and that 'inverted isograds are also observed in units proved to have a normal structural polarity.'

On the basis of detailed structural mapping in Nepal, Robinson *et al.* (2003) proposed a qualitative model of sequential emplacement of thrust sheets progressively toward the south, and sequential metamorphism of the rocks under the increased overburden of the thrust sheets. The overburden was envisioned to decrease southward due to the gradual climb of the basal Himalayan dècollement in that direction and erosional denudation of the rocks. It seems that this conceptual model would produce, as observed in our study, a close relationship between metamorphic crystallization and a dominant fabric, as well as increase of both pressure and temperature in the up-section direction. Furthermore, as discussed by Robinson *et al.* (2003), their model predicts a progressively older age of metamorphism with increasing grade, which is compatible with the age data of monazite inclusions in garnet (Catlos *et al.*, 2001).

The models of the group (d) also have the merit of producing both syn- to late-tectonic crystallization and inversion of the metamorphic sequence without requiring thermal inversion. Seismic data indicate convergence of MCT and STDS at depth. This should lead to ductile extrusion of the HHC rocks to the surface, as suggested by Grujic *et al.* (1996) and Vannay & Grasemann (2001).

To explain their observations in the Sutlej section in the western Himalayas showing increasing temperature at constant pressure, Vannay & Grasemann (2001) argued that during the subduction of the Indian plate, the isotherms were folded with a dip towards the foreland, but not necessarily inverted. During the subsequent thermal relaxation, the peak temperatures of the rocks at a constant depth increased towards the foreland. The mineralogical properties of the rocks attained at the peak temperature were preserved during subsequent cooling and exhumation of the rocks by shearing. In the Sutlej section, the rocks now exposed on the surface happened to have been derived from a constant depth, thereby producing an isobaric IMS. However, the orientation of the sampling line cannot be unique in a large orogen like Himalaya. Indeed, one should expect significant variations between different domains. Within the framework of the scenario proposed by Vannay & Grasemann (2001), we could envision that the sampling line in Sikkim had a dip towards the foreland, which is now manifested in the mineralogical properties that show increase of both pressure and temperature up section.

While the qualitative ideas presented by Vannay & Grasemann (2001) and Robinson *et al.* (2003) are appealing, it is important to analyse quantitatively how the thermal structure and particle paths might have evolved during the subduction of India. Impressive progress in this regard has been made by Jamieson and co-workers (Jamieson *et al.*, 1996, 2002; Beaumont *et al.*, 2001), who developed numerical models of the interaction of metamorphism, deformation and exhumation in large convergent orogens, and also specifically the Himalayas. These computer experiments provide important insights about the processes that might have been involved in the formation of the IMS in the Himalayas.

In their earlier model, Jamieson *et al.* (1996) showed that in a convergent orogen, material points from different initial positions at different depths would be extruded by syn-metamorphic ductile extrusion such that the rocks exposed at the surface after a certain amount of convergence would show progressively increasing metamorphic *P–T* conditions toward the foreland, and then after a certain point the pressure

would drop sharply. (Here metamorphic *P–T* condition implies peak temperature, and pressure at the peak temperature of metamorphism). However, as pointed out by Vannay & Grasemann (2001), the numerical model produced the thrust plane dipping in the opposite direction to that of the direction of subduction, which is contrary to the orientation of the MCT in the Himalayas.

In a numerical experiment (HT-6), Jamieson *et al.* (2002) produced thrusting similar to the attitude of MCT and inversion of the metamorphic isograds by channel flow and slope-dependent syn-convergent erosional denudation. There is also reversal of the apparent shear sense from normal at the top and reverse (that is in the direction of thrust) at the bottom of the channel flow. The normal shear at the top and reverse shear at the bottom may be thought to be representative of the STDS and MCT in the Himalayas. In this model there is also a progressive decrease of the magnitude of thrust-sense shear up section leading to zero shear, followed by normal shear. However, we are unable to test this model prediction in our study. As noted by Jamieson *et al.* (2002), the peak *P–T* conditions of surface rocks predicted in their model orogen are lower than those in the MCTZ. But these are consequences of model parameters, and it remains to be seen if these could be adjusted to appropriate values of the Himalayan orogen to produce the observed *P–T* pattern in Sikkim.

Beaumont *et al.* (2001) have presented similar computer experiments as Jamieson *et al.* (2002), but specifically focused on the Himalayan tectonics and metamorphism. The overall results seem to be similar to those of Jamieson *et al.* (2002), in that the numerical model produces channel flow and ductile extrusion that are dynamically linked to focused surface erosion at the edge of a plateau that is underlain by low-viscosity material. Also in this model the peak temperature of rocks increases progressively up section, while the pressure change shows a maximum.

The observed *P–T* gradient in Sikkim seems to be unique in that other studies elsewhere reported constant or decreasing pressure with increasing temperature or a pressure maximum. If this diversity of metamorphic field gradients is indeed real then a model of tectonic inversion must have the flexibility to produce this diversity. However, a mechanism of inversion by folding the isograds does not have this flexibility. It remains to be seen if these diversity of metamorphic field gradients could be produced in numerical experiments, such as those carried out by Jamieson *et al.* (2002) and Beaumont *et al.* (2001), by reasonable adjustments of the model parameters. Our study highlights the need of careful determination of peak metamorphic *P–T* conditions on the basis of judicious thermobarometric and phase equilibria analyses for developing acceptable model(s) for the origin of the IMS in the Himalayas. These studies should be coupled with detailed structural studies to determine the sense and magnitude of shear through the IMS.

ACKNOWLEDGEMENTS

This research was supported by a joint grant from the NSF International Program, INT 0002004, and the DST, Government of India, DST/INT/US(NSF-RP031)/2000. We also acknowledge the support from the Alexander von Humboldt forschungspreis (JG) and the Deutsche Forschunggemeinschaft (SD & SN) during the course of preparation of this manuscript, and providing the opportunity for close interaction by bringing all of us to the same place at the same time. We thank Drs S. Chakraborty, R. Jamieson, E. Ghent and G. Droop for critical but constructive reviews of the manuscript, Drs P. DeCelles and J.-C. Vannay for helpful discussions, and Prof. M. Brown for his editorial handling and helpful suggestions for the improvement of the manuscript.

REFERENCES

Acharya, S. K. & Shastry, M. V. A., 1979. Stratigraphy of Eastern Himalaya. *Geological Survey of India Miscellaneous Publication*, **41,** 49–67.

Applegate, J. D. R. & Hodges, K. V., 1994. Empirical evaluation of solution models for pelitic minerals and their application to thermobarometry. *Contributions to Mineralogy and Petrology*, **117,** 56–65..

Beaumont, C., Jamieson, R. A., Nguyen, M. H. & Lee, B., 2001. Himalayan tectonics explained by extrusion of a low-viscosity crystal channel coupled to focused surface denudation. *Nature*, **414,** 738–742.

Berman, R. G. & Aranovich, I. Y., 1996. Optimized standard state and solution properties of minerals. I. Model calibration for olivine, orthopyroxene, cordierite, garnet, and ilmenite in the system FeO–MgO–CaO–Al_2O_3–TiO_2–SiO_2. *Contributions to Mineralogy and Petrology*, **126,** 1–24.

Bhattacharya, D. S. & Das, K. K., 1983. Inversion of metamorphic zones in the lower Himalayas at Gangtok, Sikkim, India. *Journal of Geology*, **91,** 98–102.

Bhattacharya, A., Mohanty, L., Maji, A., Sen, S. K. & Raith, M., 1992. Non-ideal mixing in the phlogopite–annite binary: constraints from experimental data on Mg-Fe partitioning and a reformulation of biotite-garnet thermometer. *Contributions to Mineralogy and Petrology*, **111,** 87–93.

Catlos, E. J., Harrison, T. M., Kohn, M. J. *et al.*, 2001. Geochronologic and thermobarometric constraints on the evolution of the Main Central Thrust, Central Nepal, Himalaya. *Journal of Geophysical Research*, **106,** 16177–16204.

Chakraborty, S., Dasgupta, S. & Neogi, S., 2004. Mass Transfer controlled nucleation kinetics and its tectonic implications. *American Mineralogist*, in review.

England, P., LeFort, P., Molnar, P. & Pecher, A., 1992. Heat sources for Tertiary metamorphism and anatexis in the Annapurna-Manaslu region, Central Nepal. *Journal of Geophysical Research*, **97,** 2107–2128.

Ferry, J. M. & Spear, F. S., 1978. Experimental calibration of the partitioning of Fe and Mg between biotite and garnet. *Contributions to Mineralogy and Petrology*, **66,** 113–117.

Frank, W., Hoinkes, G., Miller, C., Purtscheller, F., Richter, W. & Thoeni, M., 1975. Relations between metamorphism and orogeny in a typical section of the Indian Himalayas; NW-Himalaya; S-Lahul, Kulu; Himachal Pradesh; first

comprehensive report. *Tschermaks Mineralogische Petrographische Mitteilungen*, **20,** 303–332.
Fraser, G., Worley, B. & Sandiford, M., 2000. High precision geothermobarometry across the High Himalayan metamorphic sequence, Langtang valley, Nepal. *Journal of Metamorphic Geology*, **18,** 665–681.
Fuhrman, M. L. & Lindsley, D. H., 1988. Ternary feldspar modelling and thermometry. *American Mineralogist*, **73,** 201–216.
Ganguly, J., 1969. Chloritoid stability and related parageneses: theory, experiments, and applications. *American Journal of Science*, **267,** 910–944.
Ganguly, J., 1977. Compositional variables and chemical equilibrium in metamorphism. In: *Energetics of Geological Processes* (eds Saxena, S. K. & Bhattacharya, S.), pp. 250–284.
Ganguly, J. & Saxena, S. K., 1987. *Mixtures and mineral reactions*. Springer, Berlin, 291 pp.
Ganguly, J. & Tirone, M., 1999. Diffusion closure temperature and age of a mineral with arbitrary extent of diffusion: theoretical formulations and applications. *Earth and Planetary Science Letters*, **170,** 131–140.
Ganguly, J., Bhattacharya, R. N. & Chakraborty, S., 1988. Convolution effect in the determination of compositional profiles and diffusion coefficients by microprobe step scans. *American Mineralogist*, **73,** 901–909.
Ganguly, J., Cheng, W. & Tirone, M., 1996. Thermodynamics of aluminosilicate garnet solid solution: new experimental data, an optimized model and thermometric applications. *Contributions to Mineralogy and Petrology*, **126,** 137–151.
Ganguly, J., Cheng, W. & Chakraborty, S., 1998. Cation diffusion in aluminosilicate garnets: experimental determination in pyroxene-almandine diffusion couples. *Contributions to Mineralogy and Petrology*, **131,** 171–180.
Ganguly, J., Dasgupta, S., Cheng, W. & Neogi, S., 2000. Exhumation history of a section of the Sikkim Himalaya, India: records in the metamorphic mineral equilibria and compositional zoning of garnet. *Earth and Planetary Science Letters*, **183,** 471–486.
Grujic, D., Casey, M., Davidson, C. *et al*., 1996. Ductile extrusion of the Higher Himalayan Crystalline in Bhutan: Evidence from quartz microfabrics. *Tectonophysics*, **260,** 21–43.
Hodges, K. V., 2000. Tectonics of the Himalaya and southern Tibet from two perspectives. *Geological Society of America Bulletin*, **112,** 324–350.
Hodges, K. V. & Silverberg, D. S., 1988. Thermal evolution of the greater Himalaya, Garhwal, India. *Tectonics*, **7,** 583–600.
Hoisch, T. D., 1990. Empirical calibration of six geobarometers for the mineral assemblage quartz + muscovite + biotite + plagioclase + garnet. *Contributions to Mineralogy and Petrology*, **104,** 225–234.
Holdaway, M. J., 1971. Stability of andalusite and aluminosilicate phase diagram. *American Journal of Science*, **271,** 97–131.
Holdaway, M. J., 2000. Application of new experimental and garnet Margules data to the garnet-biotite geothermometer. *American Mineralogist*, **85,** 881–892.
Holdaway, M. J., Dutrow, B. L. & Hinton, R. W., 1988. Devonian and carboniferous metamorphism in west-central Maine: the muscovite-almandine geobarometer and the staurolite problem revisited. *American Mineralogist*, **73,** 20–47.
Holland, T. J. B. & Powell, R., 1998. An internally consistent thermodynamic dataset for phases of petrological interest. *Journal of Metamorphic Geology*, **16,** 309–343.
Hubbard, M. S., 1989. Thermobarometric constraints on the thermal history of the Main Central thrust zone and Tibetan slab, eastern Nepal Himalaya. *Journal of Metamorphic Geology*, **7,** 19–30.
Hubbard, M. S., 1996. Ductile shear as a cause of inverted metamorphism: example from the Nepal Himalaya. *Journal of Geology*, **104,** 493–499.
Inger, S. & Harris, N. B. W., 1992. Tectonothermal evolution of the High Himalayan Crystalline Sequence, Langtang Valley, northern Nepal. *Journal of Metamorphic Geology*, **10,** 439–452.
Jain, A. K. & Manickavasagam, R. M., 1993. Inverted metamorphism in the intercontinental ductile shear zone during Himalayan collision tectonics. *Geology*, **21,** 407–410.
Jamieson, R. A., Beaumont, C., Hamilton, J. & Fullsack, P., 1996. Tectonic assembly of inverted metamorphic sequences. *Geology*, **24,** 839–842.
Jamieson, R. A., Beaumont, C., Nguyen, M. H. & Lee, B., 2002. Interaction of metamorphism, deformation and exhumation in large convergent orogens. *Journal of Metamorphic Geology*, **20,** 9–24.
Kohn, M. J. & Spear, F. S., 2000. Retrograde net transfer reaction insurance for pressure-temperature estimates. *Geology*, **28,** 1127–1130.
Kohn, M. J., Catlos, E. J., Ryerson, F. J. & Harrison, T. M., 2001. Pressure–temperature time path discontinuity in the main Central thrust zone, central Nepal. *Geological Society of America*, **29,** 571–574.
Koziol, A. M. & Newton, R. C., 1989. Grossular activity-composition relationships in ternary garnets determined by reversed displaced-equilibrium experiments. *Contributions to Mineralogy and Petrology*, **103,** 423–433.
Kretz, R., 1983. Symbols of rock forming minerals. *American Mineralogist*, **68,** 277–279.
Lal, R. K., Mukherjee, S. & Ackermand, D., 1981. Deformation and Barrovian metamorphism at Takdah, Darjeeling (Eastern Himalaya). In: *Metamorphic tectonites of the Himalaya* (ed. Saklani, P. S.), pp. 231–278. Today and Tomorrow Publishers, New Delhi.
LeFort, P., 1975. Himalaya: the collided range. Present knowledge about the continental arc. *American Journal of Science*, **275A,** 1–44.
McFarlane, A. M., 1995. An evaluation of the inverted metamorphic gradient at Langtang National Park, central Nepal Himalaya. *Journal of Metamorphic Geology*, **13,** 595–612.
Mukhopadhyay, B., Holdaway, M. J. & Koziol, A. . M., 1997. A statistical model of thermodynamic mixing properties of Ca–Mg–Fe^{2+} garnets. *American Mineralogist*, **82,** 165–181.
Neogi, S., Dasgupta, S. & Fukuoka, M., 1998. High *P–T* polymetamorphism, dehydration-melting, and generation of migmatites and granites in the Higher Himalayan crystalline complex, Sikkim, India. *Journal of Petrology*, **39,** 61–99.
Neogi, S., Ravikant, V. & Dasgupta, S., 2004. The Main Central Thrust dilemma: a structural-metamorphic evaluation from Sikkim Himalaya, India. *Journal of Asian Earth Sciences* (in review).
Patiño Douce, A. E., Johnston, A. D. & Rice, J. M., 1993, Octahedral excess mixing properties in biotite: a model with applications to geothermometry and geobarometry. *American Mineralogist*, **78,** 113–131.
Pêcher, A., 1989. The metamorphism in the central Himalaya. *Journal of Metamorphic Geology*, **7,** 31–41.
Powell, R. & Holland, T. J. B., 1994. Optimal geothermometry and geobarometry. *American Mineralogist*, **79,** 120–133.
Ray, K. K., 1976. A review of the geology of the Darjeeling–Sikkim Himalayas. In: *Himalayan Geological Seminar*, New Delhi, 13–17.
Ray, S. K., 2000. Culmination zones in Eastern Himalaya. *Geological Survey India Special Publications*, **55,** 85–94.
Robinson, D. M., DeCelles, P. G., Garzione, C. N., Harrison, T. M. & Catlos, E. J., 2003. Kinematic model for the Main Central thrust in Nepal. *Geology*, **31,** 359–362.
Searle, M. P., Waters, D. J., Dransfield, M. W. *et al*., 1999, Thermal and mechanical models for the structural and metamorphic evolution of the Zanskar High Himalaya. In: *Continental tectonics* (eds Mac Niocaill, C. & Ryan, P. D.), pp. 139–156. Geological Society of London, Special Publication 164.
Sinha-Roy, S., 1982. Himalayan Main Central Thrust and its implications for Himalayan inverted metamorphism. *Tectonophysics*, **84,** 197–224.
Stephenson, B. J., Waters, D. J. & Searle, M. P., 2000. Inverted metamorphism and the Mail Central Thrust: field relations

and thermobarometric constraints from the Kishtwar Window, NW Indian Himalaya. *Journal of Metamorphic Geology*, **18,** 571–590.

Swapp, M. S. & Hollister, L. S., 1991. Inverted metamorphism within the Tibetan slab in Bhutan: evidence for a tectonically transported heat source. *Canadian Mineralogist*, **29,** 1019–1041.

Treloar, P. J., Broughton, R. D., Williams, M. P., Coward, M. P. & Windley, B. W., 1989. Deformation, metamorphism and imbrications of the Indian Plate, south of the Main Mantle Thrust, north Pakistan. *Journal of Metamorphic Geology*, **7,** 111–125.

Vannay, J. C. & Grasemann, B., 1998. Inverted metamorphism in the High Himalaya of Himachal Pradesh (NW India): Phase equilibria versus thermobarometry. *Schweizerische Mineralogische und Petrographische Mitteilungen*, **78,** 107–132.

Vannay, J. C. & Grasemann, B., 2001. Himalayan inverted metamorphism and syn-convergence extension as a consequence of a general extrusion. *Geological Magazine*, **138,** 253–276.

Vannay, J. C. & Hodges, K. V., 1996. Tectonometamorphic evolution of the Himalayan metamorphic core between Annapurna and Dhaulagiri, central Nepal. *Journal of Metamorphic Geology*, **14,** 635–656.

Vannay, J. C., Sharp, Z. D. & Grasemann, B., 1999. Himalayan inverted metamorphism constrained by oxygen isotope thermometry. *Contributions to Mineralogy and Petrology*, **137,** 90–101.

Wood, B. J., Hackler, R. T. & Dobson, D. P., 1994. Experimental determination of Mn–Mg mixing in garnet, olivine and oxide. *Contributions to Mineralogy and Petrology*, **115,** 438–448.

Received 23 December 2003; revision accepted 15 March 2004.